

Spin polarons in the t - J model in an unconstrained representation

A. V. Dotsenko

*School of Physics, The University of New South Wales, Sydney 2052, Australia**

Abstract

The report discusses the slave-fermion representations of the t - J model and describes another representation, in which fermions and bosons are completely commuting and in which the properties of fermions are directly related to the properties of physical holes. For a study of the system in the new representation at half-filling, interaction of fermions with two magnons is treated in mean-field theory. The obtained effective model, in comparison to that of the usual slave-fermion representation, has an additional bare hole dispersion due to the hole moving by using quantum spin fluctuations present in the undoped antiferromagnetic ground state. The single-hole Green's function at half-filling is then found numerically using the self-consistent Born approximation. For all studied quantities good or excellent agreement with numerical data is observed in the entire parameter range, noticeably better than in the studies with the slave-fermion representation. Using the same effective model, the two-hole problem is also studied by solving numerically the Bethe-Salpeter equation with noncrossing diagrams.

I. INTRODUCTION

Much, if not most, of the progress in describing theoretically the complex physics of high-temperature superconductors and strongly correlated electrons has been achieved using numerical methods,¹ while analytical methods have been rather approximate and not often checked against numerical data. A simple and transparent analytical or semianalytical model can however be very valuable by providing physical insights for *understanding* in addition to describing the system and by being easily extendible to other problems. Currently this is the role of the so-called self-consistent Born approximation,²⁻⁵ which provides a fairly good description of the undoped t - J model. More accurately, in this method (0) the t - J model is expressed in terms of holons and bosons⁶; then (i) the boson part is solved to leading order in $1/S$ (spin-wave theory); and finally (ii) the interacting holon-boson system is solved numerically using leading-order diagrams. (For points *i* and *ii*, higher-order terms/diagrams have been analyzed by Liu and Manousakis.⁵)

In this publication I report a study of the t - J model in a different scheme. The Hilbert space of holons and bosons is expanded, so that they are no longer constrained by each other. Another important difference is that the fermionic Green's function in the expanded model corresponds directly to the Green's function of fermions in the original t - J model.

Numerical results are then obtained for the t - J model on the square lattice at half-filling. For the first and simplest stage of analysis in the new representation, it is suggested to use mean-field treatment for zero- and two-magnon terms in the Hamiltonian. The effective model obtained this way, consisting of interacting holes and spin waves, is the same as in the usual constrained representation with the constraint ignored except for the presence of a bare hole dispersion due to the hole moving by eating away spin fluctuations present in the ground state. Solving the equations of motion for one hole in the self-consistent Born approximation, I find a fairly good agreement with numerical results for all analyzed quantities, such as the bandwidth and the band structure, and for all parameter regimes. The two-hole problem is also studied using the leading-order, noncrossing diagrams, demonstrating again viability of the method albeit much less convincingly.

In the following Sec. II, I describe the discussed formulations of the t - J model. Then, in Sec. III the obtained results for single- and two-hole problems are compared against the available numerical data and against the results obtained in the usual slave-fermion representation. The report ends with a summary (Sec. IV).

II. ANALYTICAL TRANSFORMATIONS OF THE t - J MODEL

The familiar t - J Hamiltonian is

$$H_{tJ} = -t \sum_{\langle ij \rangle \sigma} (c_{i\sigma}^\dagger c_{j\sigma} + \text{H.c.}) + J \sum_{\langle ij \rangle} (\mathbf{S}_i \cdot \mathbf{S}_j - \frac{1}{4} n_i n_j), \quad (1)$$

where the notation is standard with the addition that, both here and throughout the paper, n , i , and j refer to any, spin-up, and spin-down sublattice sites, respectively (n as a subindex is not to be confused with the electron number operators n_n). The square lattice is implied, although much of the discussion is independent of this. Recently, an extra t' term describing next-nearest-neighbor hopping is usually added to the model.⁷ This study however, being mainly for demonstrative and comparative purposes, is restricted to the original t - J model Eq. (1).

The Hamiltonian Eq. (1) is written without the commonly included electron projection operators on the understanding that, instead, the Hilbert space is restricted to no double electron occupancy (see Fig. 1). It also goes without saying that the “electrons” of the t - J model are in fact Zhang-Rice singlets.⁸

A. The holon-or-spin representation of the t - J model

To disentangle the Hamiltonian, the main degrees of freedom must be identified and suitable operators introduced. Intuitively, spin fluctuations and mobile holes are the main underlying objects. It was, to the best of the author’s knowledge, Schmitt-Rink, Varma, and Ruckenstein⁶ who first proposed to represent the system as a combination of a spinless-fermion (holon) field and a boson field. In this slave-fermion representation, the electron operators are written as $c_{n\sigma} = f_n^\dagger b_{n\sigma}$ and the Hilbert space of holons f_n and bosons $b_{n\sigma}$ is constrained by $f_n^\dagger f_n + b_{n\uparrow}^\dagger b_{n\uparrow} + b_{n\downarrow}^\dagger b_{n\downarrow} = 1$.

We can think of bosons $b_{n\sigma}$ as the Schwinger bosons of some spin field \mathbf{s}_n , which in this case corresponds directly to the physical spin, $\mathbf{S}_n = \mathbf{s}_n$. This spin field \mathbf{s}_n can also be of course represented by another type of bosons, such as the bosons a_n of the Holstein-Primakoff or Dyson-Maleev transformation. The entire system is then represented in terms of operators f_n and a_n (in the normally implied case of antiferromagnetic order the bosonic operators a_n are different on the two sublattices). The Hilbert space is constrained in this case by $f_n^\dagger f_n + a_n^\dagger a_n < 2$.

Finally, the spin field \mathbf{s}_n can be present directly rather than via bosons. This corresponds to what was done in Ref. 9 and is described here in some detail since it is closer to the model presented later. The t - J model Hilbert space Fig. 1 is mapped onto the one in Fig. 2. At any site n , there can be a holon f_n and there is *always* a spin \mathbf{s}_n . A “normal,” that is containing one electron, site is thought of as having no holon, while the spin field on such site is identified with the physical electron spin, $\mathbf{s}_n = \mathbf{S}_n$ for $f_n^\dagger f_n = 0$. An empty site is considered to have one holon. The spin \mathbf{s}_n on such a site is a dummy, or a ghost—it is unphysical. We choose to make it *up* if the site is on the spin-up sublattice and *down* otherwise. This choice is arbitrary and is motivated by the Ising limit.

The relations for operators are as follows. The physical spin is $\mathbf{S}_n = (1 - f_n^\dagger f_n) \mathbf{s}_n$. The electron operators are $c_{i\uparrow} = (\frac{1}{2} + s_i^z) f_i^\dagger$ and $c_{i\downarrow} = s_i^+ f_i^\dagger$ for the spin-up sublattice and $c_{j\uparrow} = s_j^- f_j^\dagger$ and $c_{j\downarrow} = (\frac{1}{2} - s_j^z) f_j^\dagger$ for the spin-down sublattice. The t - J Hamiltonian is then in this representation (ignoring spin projection operators)

$$H_{tJ} = t \sum_{\langle ij \rangle} f_i^\dagger f_j (s_j^+ + s_i^+ + \text{H.c.}) + J \sum_{\langle ij \rangle} (1 - f_i^\dagger f_i) (\mathbf{s}_i \cdot \mathbf{s}_j - \frac{1}{4}) (1 - f_j^\dagger f_j). \quad (2)$$

Again, we have an inhomogeneous Hilbert space, in which a spin deviation and a holon cannot coexist on a site. This transformation can be generalised to $c_{n\sigma} = f_n^\dagger \hat{U}_s$, where \hat{U}_s is some spin transformation with appropriate properties.

The representations described so far constitute big progress relative to the “raw” t - J model. In such analytical representations, by use of the half-filled state as the background, most correlations present in the system are already taken into account. Due to fermion statistics, it is automatically guaranteed that not more than one holon can be on a site. However there are also problems.

(1) The first one is the constraint, which any not overly complicated wave functions can hopefully satisfy only on average. Of course, we may “get rid” of the constraint by introducing into the Hamiltonian projection operators, but then the Hamiltonian becomes complicated. It will then have some artificial complicated terms of purely “kinematic” origin.

(2) The second disadvantage is that the holon operators in these representations only approximately correspond to the original electron operators. Indeed, $c_{n\uparrow}$ is defined differently on different sublattices, so that $c_{\mathbf{k}\uparrow}$ is not the same as $f_{\mathbf{k}}^\dagger$ but rather is a combination of $f_{\mathbf{k}}^\dagger$ and $f_{\mathbf{k}-\mathbf{q}}^\dagger s_{\mathbf{q}}^-$. It is then necessary to do additional calculations to find the Green’s function of operators c_n (see Ref. 10 and also the Appendix of Ref. 3).

Physically, both points (1) and (2) are related to ground-state quantum spin fluctuations and disappear completely for a classical Néel background. In fact even for the quantum Néel background as long as *linear* spin-wave theory is used, the constraint can be formally ignored. Both problem however get quickly more dramatic as antiferromagnetic order is weakened, which is known to happen in copper oxides.

There is also a problem with analyzing the spin field by itself. Spin-wave theory is certainly only approximate and has its limitations. However that is a general problem of condensed-matter physics rather than a problem with any particular representation of the t - J model.

B. The unconstrained representation of the t - J model

It is possible to study the t - J model in a substantially different representation. The central idea is to relax the constraint, so that when there is a hole on a site the (ghost) spin on that site can have *any* value.

This is a big step. The new Hilbert space has four states per site instead of three in the original model. Instead of being able to have strictly a holon *or* a boson, we can have a holon *and/or* boson. Thus we have essentially a different, a bigger model. No one-to-one transformation is taking place. (It has in fact been claimed recently¹¹ using symmetry arguments that it is impossible to transform the t - J model to a model of commuting fermions and spins.) We may still call the new model a “representation” of the t - J model in the sense of group theory (a reducible representation). Two of the states in the new model, $|0_f, \uparrow\rangle$ and $|0_f, \downarrow\rangle$, correspond to one state in the original model, $|\cdot\rangle$. The correspondence for spin operators is as simple as before, $\mathbf{S}_n \rightarrow (1 - f_n^\dagger f_n) \mathbf{s}_n$. It is also clear that a hole remains a hole. For single-fermion operators there is however no simple relation.

We are free to define the dynamics of the ghost spin in new model—one can think of it as choosing the gauge. (The dynamics of the nonghost spin should, of course, be the same as in the original model.) For example, we can choose the hopping part of the Hamiltonian to have the following form,

$$H_t = t \sum_{\langle nn'\rangle\sigma\sigma'} (|1_f\sigma'\rangle_{n'}|0_f\sigma\rangle_n \langle 1_f\sigma'|_n \langle 0_f\sigma|_{n'} + \text{H.c.}). \quad (3)$$

Here σ is a nonghost spin, and so it should just hop without flipping. We have chosen that the ghost spin, σ' , also simply hops. The ghost spin is thus permanently attached to the hole. Note that it is important here to consider hopping as a single elementary process, not as a combination of two processes of destruction and creation of the hole.

The complete Hamiltonian, when written in terms of spin operators, is then

$$H_{fs} = 2t \sum_{\langle nn'\rangle} f_n^\dagger f_{n'} \left(\frac{1}{4} + \mathbf{s}_n \cdot \mathbf{s}_{n'} \right) + J \sum_{\langle nn'\rangle} (1 - f_n^\dagger f_n) \left(\mathbf{s}_n \cdot \mathbf{s}_{n'} - \frac{1}{4} \right) (1 - f_{n'}^\dagger f_{n'}). \quad (4)$$

The subindex fs at H emphasises that this Hamiltonian is not the t - J Hamiltonian. H_{fs} is different from H_{tJ} , it acts in a different Hilbert space, in a Hilbert space that it is not even isomorphic to the Hilbert space of the t - J Hamiltonian. Nevertheless H_{fs} has been constructed in such a way that the properties in the t - J model can be simply derived from the properties in the “ f - s ” model.

The Hamiltonian Eq. (4) has been derived by Wang and Rice.¹² However I believe that their method of derivation is doubtful and their interpretation is different in that they claim to have an exact expression of the t - J model (*i.e.* a one-to-one transformation). In any case, there have been no calculation in this representation.

The spin-fermion interaction in Eq. (4) is of a very natural form for spinless fermions. The fermion propagates either by emitting and absorbing two magnons or directly by using fluctuations present in the ground state. The opposite cases of completely antiferromagnetic and ferromagnetic order are naturally covered.

Although quite simple and very symmetric, this model is relatively difficult to study because it leads to two-magnon processes. Below, the model with ghost-spin dynamics defined in a different way will be analysed. The dynamics of the ghost spin at hopping processes is defined by the diagrams in Fig. 3. The logic behind these relatively complicated rules is clarified in Appendix A where an Ising-type situation is considered. The intention is to have two-magnon-type interaction for the relatively-infrequent interaction with ground-state fluctuations but single-magnon for creating fluctuations.

Now it is time to see if the problems (1) and (2) of the slave-fermion representation have been answered.

(1) It is important that there are now no boson-fermion constraints, the two fields are interacting dynamically but are *kinematically* completely free from each other. Their might be constraints on the bosons when the spin field \mathbf{s}_n is expressed through them. However this is a constraint, *e.g.*, from spin-wave theory and it concerns bosons alone. The new model does not solve the problem of magnetic order as such, but it does separate it from the total problem.

(2) To prove that the properties of fermions in this model are equal to the properties of holes in the t - J model, consider the following argument. Let us set *at photoemission processes* the following correspondence: $c_{n\downarrow} \rightarrow f_n^\dagger(\frac{1}{2} + s_n^z)$ and $c_{n\uparrow} \rightarrow f_n^\dagger(\frac{1}{2} - s_n^z)$ and likewise for Hermitian conjugates. That is to say that creation of a hole is represented as creation of a holon and, importantly, the spin on the site remains unchanged (we may say that it turns from a nonghost one to a ghost one). At subsequent hoppings the ghost spin changes according to the rules outlined above; the physics should be independent of this. Then we have $c_{\mathbf{k}\uparrow} + c_{\mathbf{k}\downarrow} \rightarrow f_{\mathbf{k}}^\dagger$ and it is easy to see that there will be a direct relation for Green's functions. The holon is now in *some* sense a symmetric mixture of spin-up and spin-down holes.

It should be also possible to introduce spin-carrying holes. The Hilbert space would be the direct product of the space of $f_{n\uparrow}$ and $f_{n\downarrow}$ (coexistence forbidden) and of spin \mathbf{s}_n . However it is unclear if such a version would give any advantages.

C. Deriving an effective model

At this point the Hamiltonian has only become more complicated. The important point however is that it can now be simplified significantly without loosing much accuracy. Fortunately, having numerical data allows to quickly test if this is so, at least in simple situations.

The guidance for the simplifications is that the spin fluctuations in the ground state are present in small numbers. The well-known¹³ characteristics of the Néel ground state are the staggered magnetization, $m^\dagger = |\langle \psi_{\text{Néel}} | s_n^z | \psi_{\text{Néel}} \rangle| \approx 0.305$, and the nearest-neighbor spin correlator, $e_{\text{AF}} = \langle \psi_{\text{Néel}} | \mathbf{s}_i \cdot \mathbf{s}_j | \psi_{\text{Néel}} \rangle |_{\langle ij \rangle} \approx -0.33$.

The first two processes in Fig. 3 describe the hole propagating by emitting and absorbing spin waves. These processes are the same as known for the slave-fermion scheme and I treat

them to leading order in $1/S$. The last two processes of Fig. 3 describe the hole moving “friction-free,” by using the liquid component of the Néel state. In these terms I replace spin combinations by their expectation values (*i.e.* do a mean-field/Hartree-Fock procedure where the inverse influence of the holes on the spin field is ignored). A relationship required here is

$$\langle \psi_{\text{Néel}} \left| \left(\frac{1}{2} + s_i^z \right) \left(\frac{1}{2} + s_j^z \right) + s_i^+ s_j^- \right| \psi_{\text{Néel}} \rangle = \frac{1}{4} + e_{\text{AF}}.$$

In the following, the following standard notation is used, $z = 4$ is the coordination number, N is the number of sites on the lattice, $\mathbf{Q} = (\pi, \pi)$, $\gamma_{\mathbf{k}} = \frac{1}{2}(\cos k_x + \cos k_y)$, and $\nu_{\mathbf{q}} = \left(1 - \gamma_{\mathbf{q}}^2\right)^{1/2}$.

With the described simplifications and after Fourier transformations, the effective Hamiltonian is

$$\begin{aligned} H_{\text{eff}} = & \sum_{\mathbf{k}} E^{(0)}(\mathbf{k}) f_{\mathbf{k}}^\dagger f_{\mathbf{k}} + \sum_{\mathbf{q}} \omega_{\mathbf{q}} \alpha_{\mathbf{q}}^\dagger \alpha_{\mathbf{q}} + \frac{zt}{\sqrt{N}} \sum_{\mathbf{k}\mathbf{q}} M(\mathbf{k}, \mathbf{q}) (f_{\mathbf{k}}^\dagger f_{\mathbf{k}-\mathbf{q}} \alpha_{\mathbf{q}} + \text{H.c.}) \\ & + \frac{1}{N} \sum_{\mathbf{k}\mathbf{k}'\mathbf{q}} \Gamma_{\text{cont}}(\mathbf{q}) f_{\mathbf{k}'-\mathbf{q}}^\dagger f_{\mathbf{k}+\mathbf{q}}^\dagger f_{\mathbf{k}} f_{\mathbf{k}'}. \end{aligned} \quad (5a)$$

The first term here, as a noticeable difference from the unconstrained case, is a bare fermion dispersion

$$E^{(0)}(\mathbf{k}) = \left(\frac{1}{4} - e_{\text{AF}}\right) zJ - 2 \left(\frac{1}{4} + e_{\text{AF}}\right) zt\gamma_{\mathbf{k}}. \quad (5b)$$

The next two terms, describing spin waves with dispersion $\omega_{\mathbf{q}} = \frac{1}{2}zJ\nu_{\mathbf{q}}$ and interaction between holes and spin waves, are the same as in the slave-fermion case. The vertex function can be (conveniently?) written as

$$M(\mathbf{k}, \mathbf{q}) = \left[\frac{1}{2}(\nu_{\mathbf{q}}^{-1} + 1)\gamma_{\mathbf{k}-\mathbf{q}}^2 + \frac{1}{2}(\nu_{\mathbf{q}}^{-1} - 1)\gamma_{\mathbf{k}}^2 - \nu_{\mathbf{q}}^{-1}\gamma_{\mathbf{q}}\gamma_{\mathbf{k}}\gamma_{\mathbf{k}-\mathbf{q}} \right]^{1/2}. \quad (5c)$$

The last term, with

$$\Gamma_{\text{cont}}(\mathbf{q}) = \frac{1}{2} \left(e_{\text{AF}} - \frac{1}{4} \right) zJ\gamma_{\mathbf{q}}, \quad (5d)$$

may be called a “contact” interaction as it describes instantaneous attraction of holes on hearest-neighbor sites (easily recognized to be due to the “broken-bond” mechanism). This interaction is also present in the slave-fermion case but is usually omitted since it is negligible in the usually considered regime of $J/t \ll 1$ and completely irrelevant in the single-hole problem. The effective model does not cover, obviously, the extreme Nagaoka case of $t/J \rightarrow \infty$ and the high-energy physics.

It is trivially seen that the slave-fermion model is recovered when switching off the bare hole dispersion. The linear-in- t hole dispersion in the static limit has been known for some time.¹⁴ It may be obtained directly by calculating the amplitudes

$$\left\langle \psi_{\text{Néel}} \left| c_{i\sigma}^\dagger \left(t \sum_{\sigma'} c_{j\sigma'}^\dagger c_{i\sigma'} \right) c_{j\sigma} \right| \psi_{\text{Néel}} \right\rangle,$$

and remembering to normalize hole operators. What is remarkable is that this effect can be added “linearly” to the spin-wave-emission mechanism.

III. COMPARISON OF RESULTS

A. The single-hole problem

To find the single-hole Green's function given the effective Hamiltonian Eqs. (5) it appears natural to use the same self-consistent Born approximations that has been used in the slave-fermion case. The first crossing diagram Fig. 4 is prohibited by kinematic reasons (it may be seen when the two-sublattice formalism is used that the spin wave emitted when the hole jumps from sublattice $\{i\}$ to sublattice $\{j\}$ must be absorbed when the hole jumps from sublattice $\{j\}$ back to $\{i\}$). The Green's function is then found by solving the following Dyson equation (corresponding to the diagram in Fig. 5),

$$[G(\mathbf{k}, \omega)]^{-1} = [G^{(0)}(\mathbf{k}, \omega)]^{-1} - \frac{(zt)^2}{N} \sum_{\mathbf{q}} M^2(\mathbf{k}, \mathbf{q}) G(\mathbf{k} - \mathbf{q}, \omega - \omega_{\mathbf{q}}), \quad (6)$$

where $G^{(0)}(\mathbf{k}, \omega) = [\omega - E^{(0)}(\mathbf{k}) + i0]^{-1}$ is the zeroth order Green's function and integration over spin-wave frequencies has been carried out using the observation that in the single-particle case all poles of $G(\mathbf{k}, \omega)$ are in the lower plane. (On the antiferromagnetic background, we could use the magnetic Brillouin zone, but it is more convenient to use the full one, it is however not the "true" Brillouin zone.)

In Figs. 6, 7, and 8, the solution of Eq. (6) on a 4×4 lattice is compared against exact results (I used data from Refs. 14 and 15). The agreement can be rated as good to excellent. Other quantities, such as the structure of the spectral function, were in good agreement too. Note also that since no account has been taken of small-cluster specifics, such as a slightly different magnetic order and a relatively large influence of the hole on the spin order (very roughly speaking, one hole on a 4×4 lattice constitutes a sizeable 6% doping), it may be conjectured that the method is even more accurate than may be suggested by the given comparison. That the agreement is not an artifact of the highly degenerate 4×4 lattice is proved in Fig. 9, where the dispersion relation is compared to that obtained¹⁶ by the Green's function Monte Carlo method on the 16×16 lattice. In examining the accuracy it should also be remembered that physically the low-energy part of the band is most important (the close agreement for the quasiparticle residue at the band bottom is thus most encouraging).

Since the computational load is quite low, it is easy to move on to fairly large lattices. Finite-size effects per se almost disappear starting from the 8×8 lattice. The main drawback of small clusters seems to be a lack of resolution in \mathbf{k} space (however in the case of dispersion, which is a very smooth function, it can be mostly overcome by using trigonometric-function fits).

The dispersion relation calculated on a 32×32 lattice is shown in Figs. 10 and 11. Of course, the most notable difference from previous slave-fermion studies is that there is no degeneracy between \mathbf{k} and $\mathbf{k} + \mathbf{Q}$. In the low-energy part of the band there is now an extended nearly flat region near $X = (\pi, 0)$. This is in agreement with the experimental angle-resolved photoemission spectroscopy (ARPES) data and is probably key to explaining some of the experimental properties of the cuprates.¹⁷

Another effect observed in the results is that the band minimum slightly shifts away from $\bar{M} = (\pi/2, \pi/2)$ towards $M = (\pi, \pi)$ while the maximum splits, moving from $\Gamma = (0, 0)$ in the

direction of $X = (\pi, 0)$ and Y . Using various lattices and supplementing it with interpolation by means of trigonometric-functions fits, I found the minimum to be at $(0.503\pi, 0.503\pi)$ for $J/t = 0.4$ and at $(0.545\pi, 0.545\pi)$ for $J/t = 1$.

Higher-order terms will probably lead to a renormalization of the values of t and J , similar to what was found in the slave-fermion case.⁵ In the present study, the shape of the dispersion is almost the same in a fairly wide parameter range and is presumably very accurate but the absolute numbers may change.

B. The two-hole problem

As a further test of the method's usefulness, I applied it to the two-hole problem. Many issues that come up here are the same as in the many-body problem and, again, availability of some numerical data makes it a good opportunity to test viability and/or accuracy of the diagrammatic approach in a context more complex than the single-particle one. To the best of the author's knowledge, no such test has been made in the framework of the slave-fermion approach either and I believe this problem must be definitively solved analytically before attacking the many-body problem. All the following consideration is restricted to pairs with total momentum zero.

The bound state is found by solving the Bethe-Salpeter equation

$$G_{\uparrow\downarrow}(\mathbf{k}, \omega) = \frac{1}{2\pi N} \sum_{\mathbf{k}'} \int d\omega' V(\mathbf{k}, \mathbf{k}', \omega - \omega') G(\mathbf{k}', E + \omega') G(-\mathbf{k}', E - \omega') G_{\uparrow\downarrow}(\mathbf{k}', \omega'), \quad (7)$$

where E is half the total energy (*i.e.* the energy *per hole*). The function $G_{\uparrow\downarrow}(\mathbf{k}, \omega)$ appears from decoupling the four-particle hole Green's function at the bound state. It corresponds to the anomalous Green's function in the many-body (Eliashberg) problem and to the pair wave function (in momentum space) in the limit of static hole-hole interaction. For the four-particle scattering amplitude I used

$$V(\mathbf{k}, \mathbf{k}', \omega) = (zt)^2 M(\mathbf{k}, \mathbf{k} - \mathbf{k}') M(\mathbf{k}', \mathbf{k}' - \mathbf{k}) D(\mathbf{k} - \mathbf{k}', \omega) + \Gamma_{\text{cont}}(\mathbf{k} - \mathbf{k}'),$$

where $D(\mathbf{q}, \omega) = 2\omega_{\mathbf{q}}(\omega^2 - \omega_{\mathbf{q}}^2 + i0)^{-1}$ is the magnon Green's function. Note that the product of M 's is simply $[\gamma_{\mathbf{k}}\gamma_{\mathbf{k}'} - \frac{1}{2}\gamma_{\mathbf{q}}(\gamma_{\mathbf{k}}^2 + \gamma_{\mathbf{k}'}^2)]\nu_{\mathbf{q}}^{-1}$. This amplitude corresponds to the leading-order spin-wave exchange diagram and the contact interaction, which is all diagrammatically represented in Fig. 12.

In solving Eq. (7), the convolution over frequencies was performed using fast Fourier transforms (FFT), taking in various regimes 1024 to 8192 points for the frequency mesh. The frequency cutoff was typically $8t + 3J$. Although despite appearances the structure of the vertex allows FFT over momenta as well, doing so in practice involves fairly large overheads and small lattices are solved faster by direct summation in \mathbf{k} space, using all available symmetries. The bound state energy is found as the E at which (the real part of) the largest eigenvalue for a given symmetry becomes equal to 1 (the imaginary part was kept under 0.05 and its negligible influence was verified). The binding energy per pair is then $\Delta_B = 2(E - E_{\text{min}})$, where E_{min} is the minimum single-hole energy (for consistency, this must be found from the momenta actually available on the cluster instead of by interpolation or by using the bulk limit result).

The solution I consider is even in frequency and has a $d_{x^2-y^2}$ -wave spatial symmetry. The results, presented in Fig. 14, show a maybe-satisfactory agreement with numerical data. The dependence of binding energy on J/t is noticeably different. The size dependence is however matched rather well, suggesting that the difference is due to a “renormalization.” This is further illustrated in Fig. 15, where the result for obtained on the 16×16 lattice is also plotted, demonstrating almost complete finite-size convergence at such sizes.

Barring the possibility of an error, the most likely cause of the discrepancy is contribution of higher-order diagrams.²⁰ In the regime of small t/J , the calculated binding energy behaves as square of the quasiparticle residue, which is what is expected but which is not what is seen in numerical data. The small size of the bound state may mean that a real-space based approach may be more efficient as the complexity of diagrams grows very quickly. The next-order omitted diagrams are shown in Fig. 13. The first crossing diagram, however, is expected to be zero for the same kinematic reason as in the single-hole case.²¹

Note also that the binding energy is quite small relative to the total energy scale. The result is very sensitive to values of interaction and the values of single-hole energy. Given the complexity of the problem, renormalizing the interaction is an attractive option.

Various features of the two-hole bound state have been discussed at length in the literature (see Ref. 1 and references therein, recent references are Refs. 22, 23, and the very detailed Ref. 24) and will not be described here except for a note on the “static” nature of the bound state. In the most naive, “nonrelativistic” static limit the spin-wave Green’s function is replaced by $-2\omega_{\mathbf{q}}^{-1}$, thus creating a potential interaction. A more accurate approximation is to take into account holes’ velocity but assume a static Green’s function, $G_{\uparrow\downarrow}(\mathbf{k}, \omega) = G_{\uparrow\downarrow}(\mathbf{k}, \omega = 0) \equiv \Psi(\mathbf{k})$. This approach, used in several studies of the t - J model,²⁵ is based on the following argument. Since the vertex function $M(\mathbf{k}, \mathbf{q})$ is small for small q , magnons with small momentum are not important in the problem. The *typical* energy of magnons involved in spin-wave exchange is of the order of $2J$. On the other hand, the energy scale for holes excitations is $\frac{1}{2}(|\Delta_B| + W_{\text{eff}})$, where the effective hole bandwidth is $W_{\text{eff}} \sim 0.3t$, so that even at $J/t \sim 0.4$ the holes may be regarded as very slow. Mathematically it means that in the range in which $G(\mathbf{k}, E + \omega)G(-\mathbf{k}, E - \omega)$ is not negligible, the function $G_{\uparrow\downarrow}(\mathbf{k}, \omega)$ does not change much, so that for integration in Eq. (7) one can replace $G_{\uparrow\downarrow}(\mathbf{k}, \omega)$ with $G_{\uparrow\downarrow}(\mathbf{k}, 0)$. The results of solving the static version of the Bether-Salpeter equation,

$$\Psi(\mathbf{k}) = \frac{1}{2\pi N} \sum_{\mathbf{k}'} \int d\omega' V(\mathbf{k}, \mathbf{k}', -\omega') G(\mathbf{k}', E + \omega') G(-\mathbf{k}', E - \omega') \Psi(\mathbf{k}'), \quad (8)$$

at $J/t = 0.4$ are shown in Fig. 15. They show that the static approximation, of course far from being completely safe, should be sufficient for most estimations, especially considering that errors introduced this way seem to be less than those originating from other sources (presumably from neglecting or mean-field-decoupling higher-order diagrams).

IV. SUMMARY

I have analysed the t - J model using an “unconstrained” representation, in which fermions and bosons are fully commuting and in which fermions correspond closer to the fermions

in the original t - J model. The results for single-hole properties within noncrossing-diagram approximation have been found to be in good agreement with numerical data. The results clarify the nature of the hole dynamics. It is almost completely described by only two kinds of underlying processes: (*i*) a string-picture-like motion by means of emitting/absorbing a spin wave at each step and (*ii*) direct hopping on ground-state spin fluctuations. The results for the two-hole problem are less clear and more work may be required.

In the physical regime of small J/t and on antiferromagnetic background, the numerical differences of the slave-fermion formulation, from the presented method are fairly small. However since the described method has exactly the same level of complexity (or rather simplicity), there is no reason not to use it. It is also important that this representation has the potential to be used on a background with an arbitrary magnetic order.

ACKNOWLEDGMENTS

The author's work was supported from an Australian Research Council grant. Part of the work was performed at das Max-Planck-Institut für Physik komplexer Systeme in Dresden, Germany.

APPENDIX A: THE MOTION OF A HOLE ON AN ISING-TYPE BACKGROUND

In this Appendix I describe the hole motion in the presence of ground-state spin fluctuations using a very simple one-dimensional Ising system. In the following, all spin-down-sublattice sites have been rotated by π .

The perfect antiferromagnetic ground state is shown in Fig. 16, and the motion of a hole in such a background is depicted in Fig. 17. As the hole moves, it leaves behind a trail of flipped spins (in one dimension they all amount to one spin-order distortion at the origin). The hole may move back to wipe out the distortion it created. In the corresponding two-dimensional, string picture, the hole creates a spin distortion at *each* step away from the origin. The hole moves by either emitting a spin wave or by absorbing one that it has created earlier. The spin wave can be thought of as a complex-spread-out-in-space form of spin flip/distortion, conceptually the two are the same. Notice that the ghost spin field on the hole site is left effectively idle, always being nonflipped according to the convention.

Now assume that for whatever reason (perhaps due to a kind of frustration) the ground state has the form in Fig. 18, that is it has spin flips/fluctuations frozen in it (incidentally, the flips come in pairs). On this background, in addition to the processes shown earlier in Fig. 17, there will be occasional processes where the hole moves without creating any new spin distortions, but only shifting those already present (Fig. 19). Analyzing the process in Fig. 19, an inconvenience of the holon approach becomes obvious. Namely, it is that although no actual spin excitation was created, there is a spin flip in the spin field due to rigidity of the ghost spin attached to the holon. This makes the analytical transformation unnatural and it will be hard to account for such processes accurately. The easy way out is to fully employ the ghost spin by forcing it flip when necessary, thus carrying much more information and doing much more work. Figure 20 illustrates the motion of a hole

as described by the new conventions. The direction of the ghost spin effectively indicates whether any encountered spin flip could have been created by the hole back in time or if it is a background spin fluctuation. In the latter case, the hole advances to the next site free—no strings attached.

REFERENCES

- * Now at Max-Planck-Institut für Physik komplexer Systeme, Nöthnitzer Str. 38, D-01187 Dresden, Germany. Electronic address: avd@mpipks-dresden.mpg.de.
- ¹ E. Dagotto, Rev. Mod. Phys. **66**, 763 (1994).
- ² C. L. Kane, P. A. Lee, and N. Read, Phys. Rev. B **39**, 6880 (1989).
- ³ G. Martínez and P. Horsch, Phys. Rev. B **44**, 317 (1991).
- ⁴ F. Marsiglio, A. E. Ruckenstein, S. Schmitt-Rink, and C. Varma, Phys. Rev. B **43**, 10882 (1991).
- ⁵ Z. Liu and E. Manousakis, Phys. Rev. B **44**, 2414 (1991); Phys. Rev. B **45**, 2425 (1992); Phys. Rev. B **51**, 3156 (1995). I am grateful to M. Boninsegni for pointing out the last of these references.
- ⁶ S. Schmitt-Rink, C. M. Varma, and A. E. Ruckenstein, Phys. Rev. Lett. **60**, 2793 (1988).
- ⁷ O. K. Andersen, A. I. Liechtenstein, O. Jepsen, and F. Paulsen, J. Phys. Chem. Solids **56**, 1573 (1995).
- ⁸ F. C. Zhang and T. M. Rice, Phys. Rev. B **37**, 3759 (1988).
- ⁹ J. L. Richard and V. Yu. Yushankhai, Phys. Rev. B **47**, 1103 (1993).
- ¹⁰ O. P. Sushkov, G. Sawatzky, R. Eder, and H. Eskes, preprint [cond-mat/9702002](#).
- ¹¹ E. Kochetov and V. Yarunin, Phys. Rev. B **56**, 2703 (1997).
- ¹² Y. R. Wang and M. J. Rice, Phys. Rev. B **47**, 1103 (1994).
- ¹³ E. Manousakis, Rev. Mod. Phys. **63**, 1 (1991).
- ¹⁴ E. Dagotto *et al.*, Phys. Rev. B **41**, 9049 (1990).
- ¹⁵ T. Barnes, A. E. Jacobs, M. D. Kovarik, and W. G. Macready, Phys. Rev. B **45**, 256 (1992).
- ¹⁶ M. Boninsegni, Phys. Lett. A **188**, 330 (1994).
- ¹⁷ E. Dagotto, A. Nazarenko, and M. Boninsegni, Phys. Rev. Lett. **73**, 728 (1994).
- ¹⁸ T. Barnes and M. D. Kovarik, Phys. Rev. B **42**, 6159 (1990).
- ¹⁹ M. Boninsegni and E. Manousakis, Phys. Rev. B **47**, 11897 (1993).
- ²⁰ Another potential reason for discrepancy is more subtle. Consider for example the case of $J/t \rightarrow 0$. In solving the problem analytically, it is easy to generate a very large number of virtual spin waves, while in fact physically it is clear that the number has to be less than the number of lattice sites. The diagrammatic approach is inherently for the bulk limit, which means that a direct comparison is not always possible. The actual criterion for agreement should be then that when no finite size effects are found in numerical data, then the results must agree. Otherwise the procedure is undefined, and some conclusions can only be drawn indirectly.
- ²¹ This observation is due to O. Sushkov.
- ²² S. R. White and D. J. Scalapino, preprint [cond-mat/9605143](#).
- ²³ V. I. Belinicher, A. L. Chernyshev, and V. A. Shubin, Phys. Rev. B **56**, 3381 (1997).
- ²⁴ J. Riera and E. Dagotto, preprint [cond-mat/9708185](#).
- ²⁵ M. Y. Kuchiev and O. P. Sushkov, Physica C **218**, 197 (1993); Phys. Rev. B **52**, 12977 (1995); V. I. Belinicher, A. L. Chernyshev, A. V. Dotsenko, and O. P. Sushkov, Phys. Rev. B **51**, 6076 (1995). Note that in these works $h_{\mathbf{k}\sigma}$ denotes a quasiparticle operator.

FIGURES

FIG. 1. The Hilbert space in the t - J model. The arrows represent electrons.

FIG. 2. The Hilbert space in the t - J model as represented in the slave-fermion formulation. The arrows represent the spin field \mathbf{s}_n , while the circles show holons. Note that the last two configurations are on certain sublattices.

FIG. 3. Graphical representation of the hopping part of the Hamiltonian in the unconstrained model (the sublattice-unsymmetric version).

FIG. 4. The leading-order crossing diagram for the single-hole Green's function. i and j are sublattice indices.

FIG. 5. The Dyson equation for the single-hole Green's function in the self-consistent Born approximation.

FIG. 6. Quasiparticle bandwidth W on a 4×4 lattice.

FIG. 7. Quasiparticle band structure on a 4×4 lattice. The lines are trigonometric-function fits to the points plotted. The notation is in the previous figure. See Fig. 6 for the actual scale. Note there is no degeneracy between \mathbf{k} and $\mathbf{k}+\mathbf{Q}$ observed for holons. Except for $J/t = 2$, the results of the present study are almost indistinguishable from the exact ones.

FIG. 8. The quasiparticle residue Z at the point $\bar{M} = (\pi/2, \pi/2)$ on a 4×4 lattice.

FIG. 9. Quasiparticle band structure at $J/t = 0.4$ on a 16×16 lattice. The solid line (the result of the present work) was smoothed by constructing a trigonometric-function fit and it passes through all the points actually calculated. The real scales are somewhat different, $E(\Gamma) - E(\bar{M}) = 1.18t = 2.95J$ for the Green's function Monte Carlo result¹⁶ and $E(\Gamma) - E(\bar{M}) = 0.83t = 2.08J$ for the result of the present study.

FIG. 10. The quasiparticle band structure at representative values of J/t . The result was obtained using a 32×32 lattice. The actual scales are as follows. For $J/t = 0.2$, $E(\Gamma) - E(\bar{M}) = 0.45t$; for $J/t = 0.4$, $E(\Gamma) - E(\bar{M}) = 0.83t$; for $J/t = 1$, $E(\Gamma) - E(\bar{M}) = 1.40t$. See also Fig. 11.

FIG. 11. A three-dimensional plot of the “normalized” dispersion at $J/t = 0.4$.

FIG. 12. The diagrams included in the four-particle scattering amplitude $V(\mathbf{k}, \mathbf{k}', \omega)$. The next-order omitted diagrams are shown in the following Fig. 13.

FIG. 13. The higher-order diagrams for the four-particle scattering amplitude. Both diagrams are expected to be suppressed (see the text).

FIG. 14. The two-hole binding energy Δ_B as a function of t/J . The numerical results on the 4×4 lattice are from exact diagonalizations. The numerical results on the 8×8 lattice are from Monte Carlo studies (Barnes and Kovarik¹⁸ for $t/J = 0$ and Boninsegni and Manousakis¹⁹ for the other points). The numerical result on the 6×8 lattice was quoted by White and Scalapino²² in a density matrix renormalization group study. The analytical result is from Ref. 23. The irregularities at small t/J on the 4×4 lattice are caused by level crossings (at $t/J = 0.4814$ and 0.1526 , see Ref. 15).

FIG. 15. Size dependence of the two-hole binding energy Δ_B at $J/t = 0.4$. $L \times L$ is the lattice size. The dotted line is the result obtained using the static approximation described in the text.

FIG. 16. The perfectly antiferromagnetic ground state. In this and following figures half of the spins have been rotated by π .

FIG. 17. Motion of a holon in perfectly antiferromagnetic background.

FIG. 18. An antiferromagnetic ground state with spin fluctuations present.

FIG. 19. Motion of a holon encountering a ground-state spin fluctuation.

FIG. 20. Motion of a hole in a background with spin fluctuations, as appearing in the unconstrained representation.

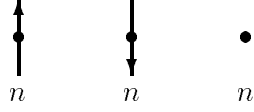


Figure 1:

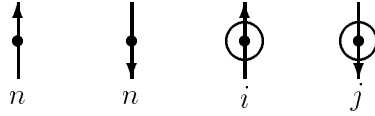


Figure 2:

a \rightleftharpoons $tf_j^\dagger f_i s_i^- \left(\frac{1}{2} - s_j^z\right) + \text{H.c.}$

b \rightleftharpoons $tf_j^\dagger f_i \left(\frac{1}{2} - s_i^z\right) s_j^+ + \text{H.c.}$

c \rightleftharpoons $tf_j^\dagger f_i \left(\frac{1}{2} + s_i^z\right) \left(\frac{1}{2} + s_j^z\right) + \text{H.c.}$

d \rightleftharpoons $tf_j^\dagger f_i s_i^+ s_j^- + \text{H.c.}$

Figure 3:

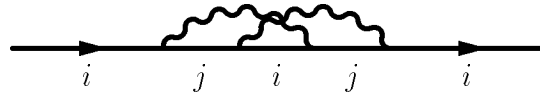


Figure 4:

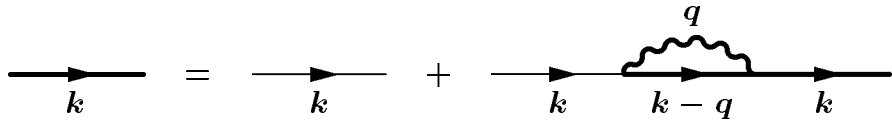


Figure 5:

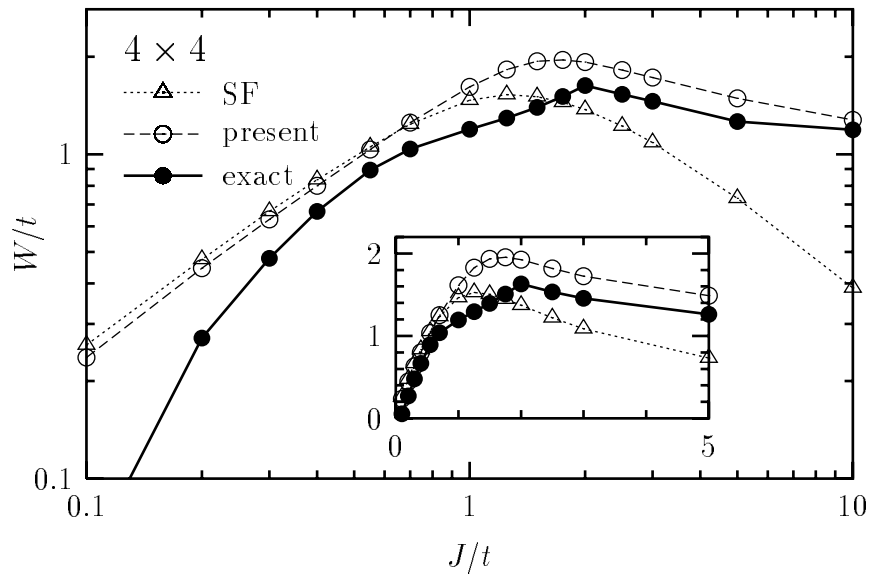


Figure 6:

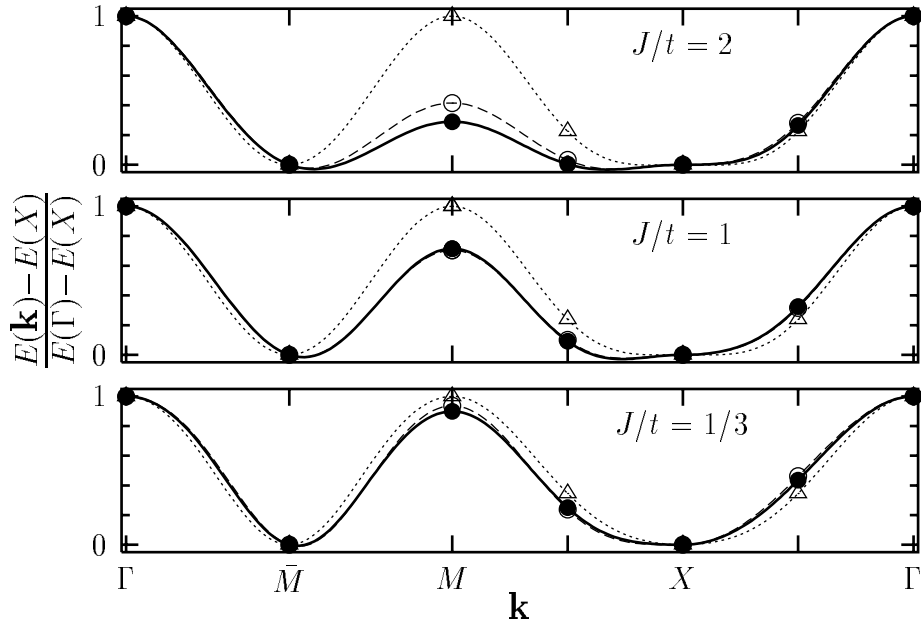


Figure 7:

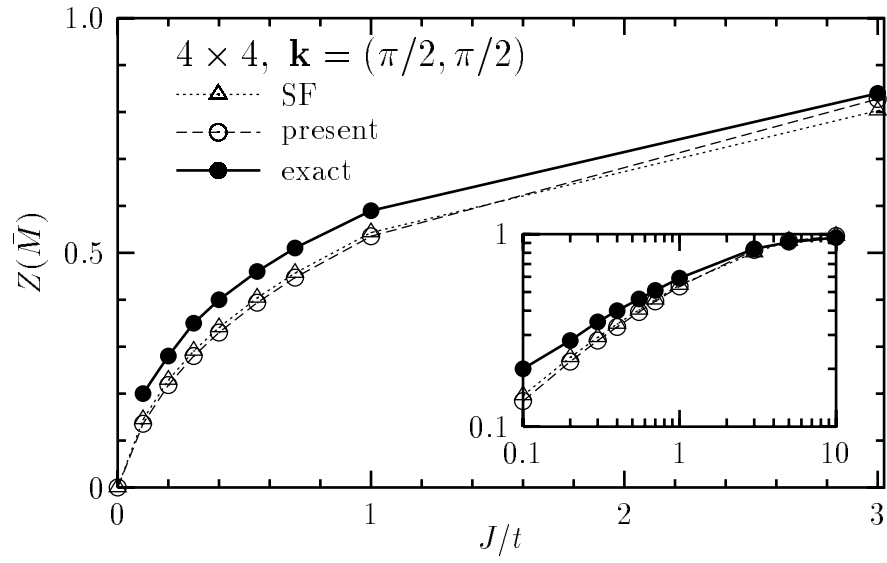


Figure 8:

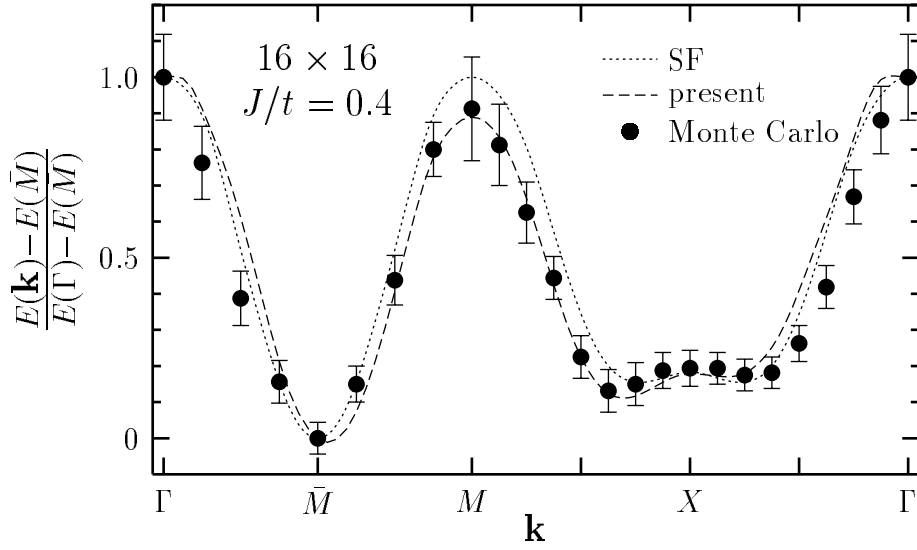


Figure 9:

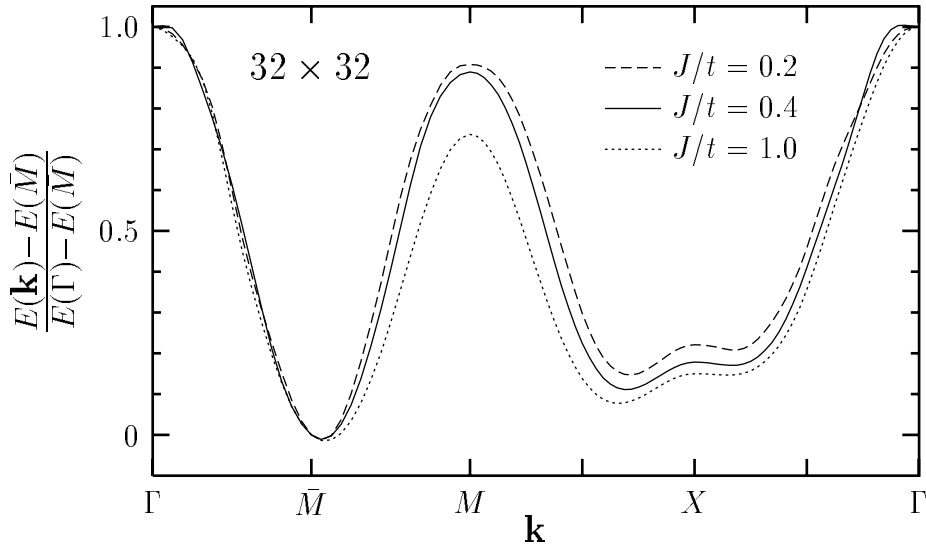


Figure 10:

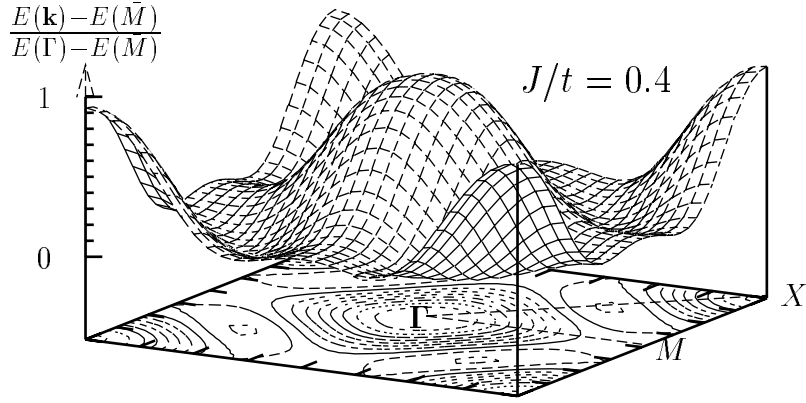


Figure 11:

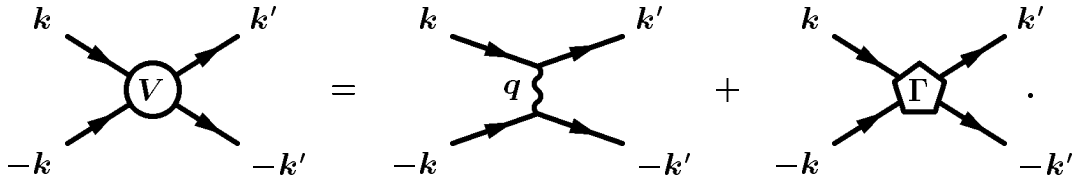


Figure 12:

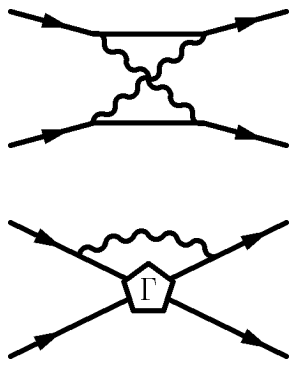


Figure 13:

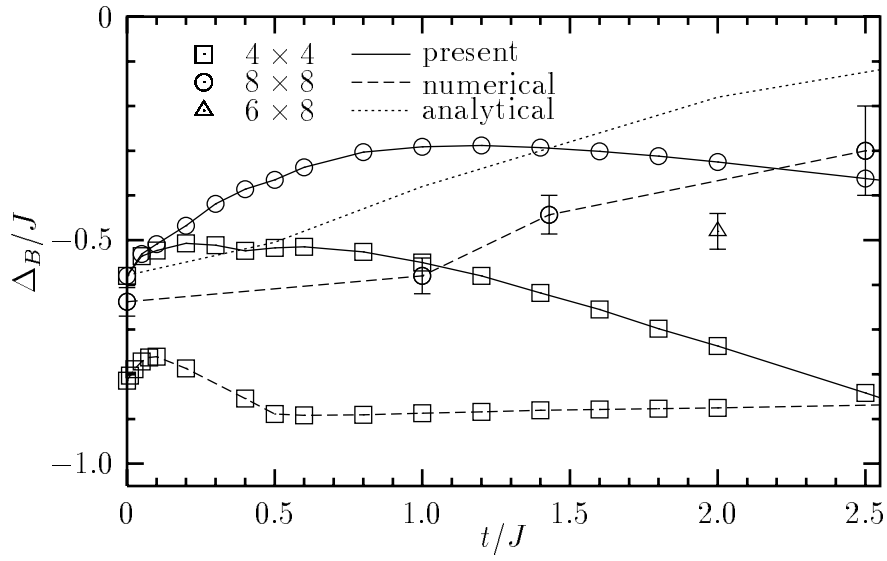


Figure 14:

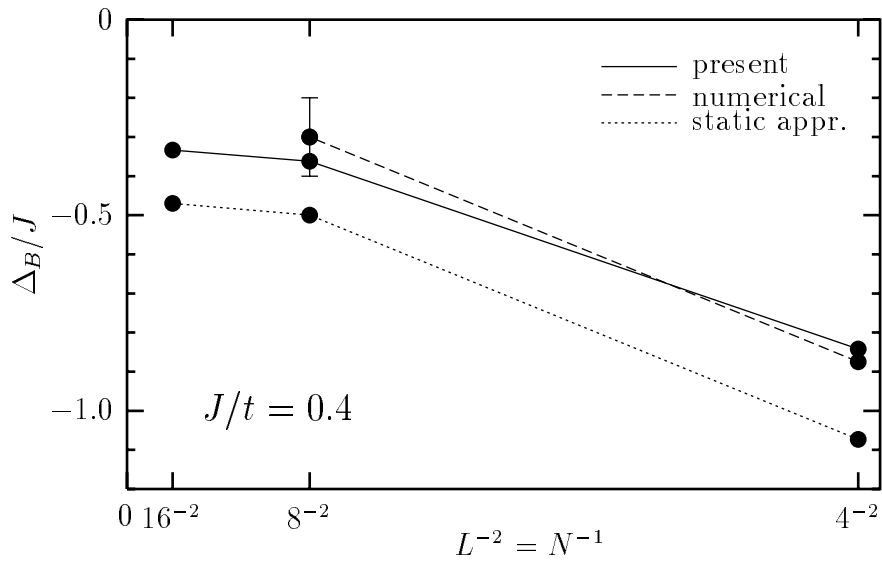


Figure 15:

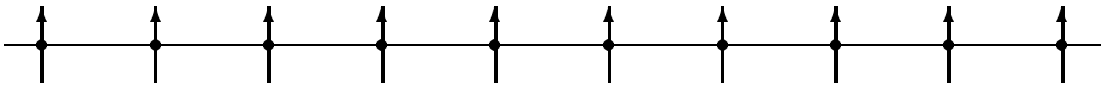


Figure 16:

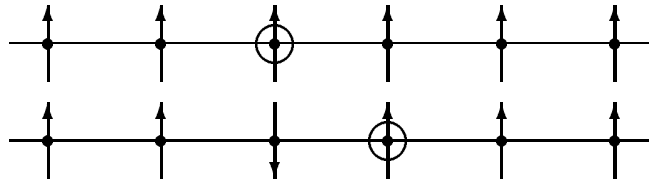


Figure 17:

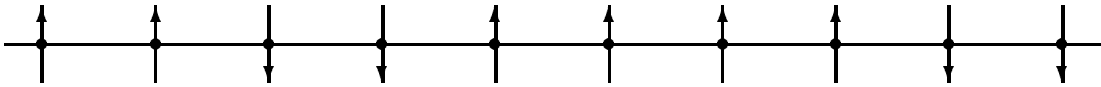


Figure 18:

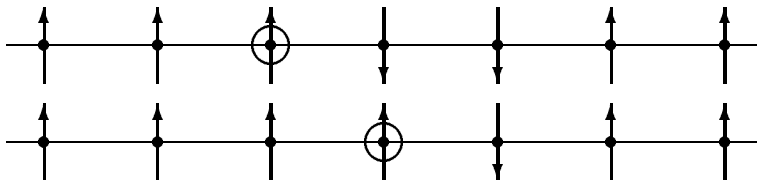


Figure 19:

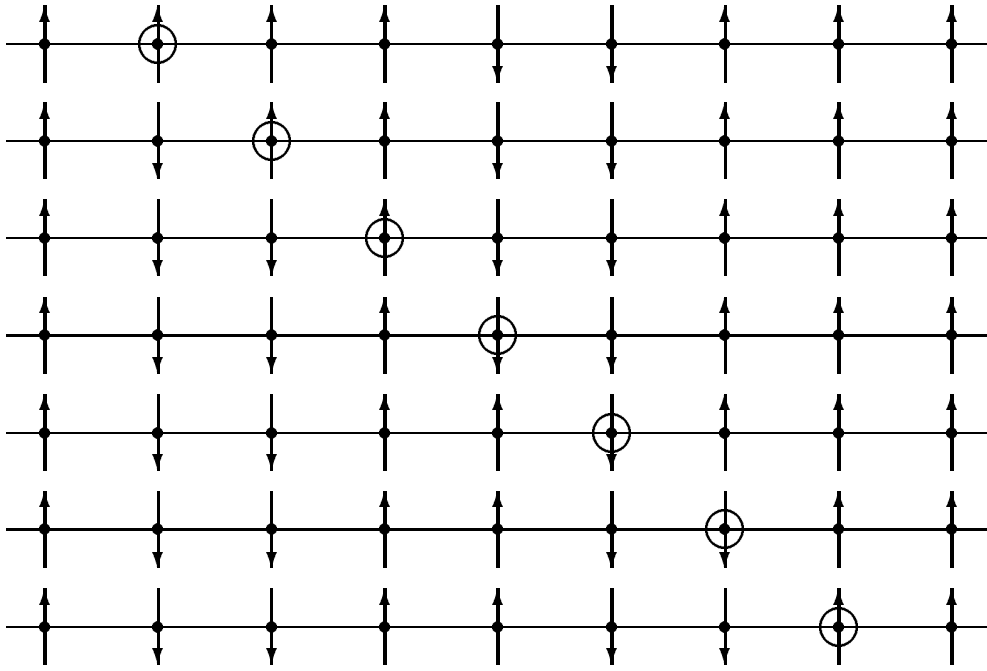


Figure 20: